# Functional Modules and Structural Basis of Conformational Coupling in Mitochondrial Complex I

Carola Hunte *et al.*

*Science* **329**, 448 (2010);
DOI: 10.1126/science.1191046



*Science* (print ISSN 0036-8075; online ISSN 1095-9203) is published weekly, except the last week in December, by the American Association for the Advancement of Science, 1200 New York Avenue NW, Washington, DC 20005. 

**References and Notes**

1. R. Jaenisch, A. Bird, *Nat. Genet.* **33**, 245 (2003).
2. M. M. Suzuki, A. Bird, *Nat. Rev. Genet.* **9**, 465 (2008).
3. R. Lister *et al.*, *Nature* **462**, 315 (2009).
4. R. A. Irizarry *et al.*, *Nat. Genet.* **41**, 178 (2009).
5. M. Okano, D. W. Bell, D. A. Haber, E. Li, *Cell* **99**, 247 (1999).
6. E. Li, T. H. Bestor, R. Jaenisch, *Cell* **69**, 915 (1992).
7. S. Nguyen, K. Meletis, D. Fu, S. Jhaveri, R. Jaenisch, *Dev. Dyn.* **236**, 1663 (2007).
8. M. Chahrour, H. Y. Zoghbi, *Neuron* **56**, 422 (2007).
9. J. Feng, H. Chang, E. Li, G. Fan, *J. Neurosci. Res.* **79**, 734 (2005).
10. H. Suh, W. Deng, F. H. Gage, *Annu. Rev. Cell Dev. Biol.* **25**, 253 (2009).
11. Materials and methods are available as supporting material on *Science* Online.
12. M. Kaneda *et al.*, *Nature* **429**, 900 (2004).
13. T. Chen, N. Tsujimoto, E. Li, *Mol. Cell. Biol.* **24**, 9048 (2004).
14. J. Otani *et al.*, *EMBO Rep.* **10**, 1235 (2009).
15. A. Meissner *et al.*, *Nature* **454**, 766 (2008).
16. D. A. Lim *et al.*, *Nature* **458**, 529 (2009).
17. R. R. Waclaw *et al.*, *Neuron* **49**, 503 (2006).
18. S. K. Ooi *et al.*, *Nature* **448**, 714 (2007).
19. M. Weber *et al.*, *Nat. Genet.* **39**, 457 (2007).
20. R. Straussman *et al.*, *Nat. Struct. Mol. Biol.* **16**, 564 (2009).
21. E. N. Gal-Yam *et al.*, *Proc. Natl. Acad. Sci. U.S.A.* **105**, 12979 (2008).
22. A. M. Lindroth *et al.*, *PLoS Genet.* **4**, e1000145 (2008).
23. R. Cao *et al.*, *Science* **298**, 1039 (2002); published online 26 September 2002 (10.1126/science.1076997).
24. A. Smallwood, P. O. Estève, S. Pradhan, M. Carey, *Genes Dev.* **21**, 1169 (2007).
25. K. Jepsen *et al.*, *Nature* **450**, 415 (2007).
26. E. Viré *et al.*, *Nature* **439**, 871 (2006).
27. M. Rush *et al.*, *Epigenetics* **4**, 404 (2009).
28. K. D. Robertson, *Nat. Rev. Genet.* **6**, 597 (2005).



29. We thank M. Carey (UCLA) for technical assistance on in vitro chromatin recruitment assays and J. Rubenstein (University of California San Francisco) for providing the pCAG-Dlx2 expression plasmid. This work was supported by NIH RO1 grants to Y.E.S. All microarray data are deposited in Gene Expression Omnibus (www.ncbi.nlm.nih.gov/geo/) under accession number GSE22476.


**Supporting Online Material**

www.sciencemag.org/cgi/content/full/329/5990/444/DC1
Materials and Methods
SOM Text
Figs. S1 to S18
Tables S1 and S2
References


5 April 2010; accepted 3 June 2010
10.1126/science.1190485


# Functional Modules and Structural Basis of Conformational Coupling in Mitochondrial Complex I


**Carola Hunte,[1,2,3]* Volker Zickermann,[4]* Ulrich Brandt[4]†**



**Proton-pumping respiratory complex I is one of the largest and most complicated membrane protein complexes. Its function is critical for efficient energy supply in aerobic cells, and malfunctions are implicated in many neurodegenerative disorders. Here, we report an x-ray crystallographic analysis of mitochondrial complex I. The positions of all iron-sulfur clusters relative to the membrane arm were determined in the complete enzyme complex. The ubiquinone reduction site resides close to 30 angstroms above the membrane domain. The arrangement of functional modules suggests conformational coupling of redox chemistry with proton pumping and essentially excludes direct mechanisms. We suggest that a ~60-angstrom-long helical transmission element is critical for transducing conformational energy to proton-pumping elements in the distal module of the membrane arm.**


Mitochondrial complex I [proton-pumping NADH (the reduced form of nicotinamide adenine dinucleotide):ubiquinone oxidoreductase] is a macromolecular membrane complex of close to one million daltons with a central function in energy metabolism (*1*). It is the entry point for electrons from NADH into the respiratory chain, and it couples electron transfer to ubiquinone with vectorial proton pumping across the inner mitochondrial membrane. With a stoichiometry of four protons to two electrons ($4H^+/2e^-$), it contributes about 40% of the proton motive force that drives adenosine 5′-triphosphate (ATP) synthesis by ATP synthase (*2*, *3*). Complex I is a source for deleterious reactive oxygen species (ROS) (*4*, *5*) and has been implicated in the pathogenesis of a variety of neurodegenerative diseases such as Parkinson's disease, Alzheimer's disease, and Leigh syndrome (*6*, *7*). Moreover, ROS generation by complex I may contribute to aging processes (*8*).

Despite the important physiological role of complex I, its molecular mechanism of energy conversion is essentially unknown. Progress in understanding complex I function has been severely limited by the lack of detailed structural information. Electron microscopy (EM) shows an L-shaped overall architecture with a membrane arm and a hydrophilic peripheral arm that protrudes into the mitochondrial matrix (*9*, *10*) (Fig. 1A). The x-ray structure of the peripheral arm from a bacterial complex I was determined (*11*, *12*).

The peripheral arm consists of two functional modules (*1*) and comprises all redox active cofactors (*11*). The N module contains the NADH oxidation site with one flavin mononucleotide (FMN) molecule as the primary electron acceptor, whereas the Q module contains the ubiquinone reduction site (Fig. 1A). Fast electron transfer between the two catalytic sites (*13*) is mediated by a chain of seven iron-sulfur clusters. An additional iron-sulfur cluster localized near the FMN cofactor may serve a special function in protection against ROS formation (*13*–*15*). The membrane arm or P module harbors the proton-pumping machinery (*16*), presumably involving the three subunits—ND2, ND4, and ND5—that are homologous to sodium-proton antiporters (*17*).

Complex I is substituted by alternative enzymes in the widely used model organism *Saccharomyces cerevisiae*. Therefore, we have established the aerobic yeast *Yarrowia lipolytica* as a genetic model system to study eukaryotic complex I (*18*). In the complex from this source, 40 different subunits were identified with a total mass of 946.5 kD (*19*, *20*). Fourteen central subunits are highly conserved among eukaryotes and prokaryotes (*1*). They form the structural core of the two arms of the complex and are essential for its bioenergetic functions. Twenty-six accessory subunits that are not found in prokaryotes are arranged around this core and presumably function in assembly, stabilization, regulation, and additional metabolic pathways that are not directly linked to energy conservation.

Here we report the x-ray crystallographic analysis of complete *Y. lipolytica* complex I (*21*). Phase information was obtained with anomalous data of a heavy atom cluster derivative and with native data (table S1). The molecule is L-shaped, with an angle between the two arms of about 100° (Fig. 1B). The membrane arm has a length of ~180 Å, and the distance between the tip of the peripheral arm and the bottom of the membrane arm is ~190 Å. At a resolution of 6.3 Å, many secondary structure elements and especially α-helical transmembrane segments were clearly recognized in the electron density.

The positions of all eight iron-sulfur cofactors were localized in the peripheral arm by anomalous Fourier analysis (Fig. 1B and table S1). The distances between the iron-sulfur clusters are similar to those reported for the hydrophilic fragment of bacterial complex I (*15*). Seven of these clusters constitute a continuous electron wire between the catalytic sites. Manual superimposition with the partial bacterial structure based on the


[1]Institute for Biochemistry and Molecular Biology, Centre for Biological Signalling Studies (BIOSS), University of Freiburg, D-79104 Freiburg, Germany. [2]Institute of Membrane and Systems Biology, University of Leeds, Leeds LS2 9JT, UK. [3]Department of Molecular Membrane Biology, Max Planck Institute of Biophysics, D-60438 Frankfurt am Main, Germany. [4]Molecular Bioenergetics Group, Medical School, Cluster of Excellence Frankfurt "Macromolecular Complexes," Center for Membrane Proteomics, Goethe-University, D-60596 Frankfurt am Main, Germany.

*These authors contributed equally to this work.
†To whom correspondence should be addressed. E-mail: brandt@zbc.kgu.de

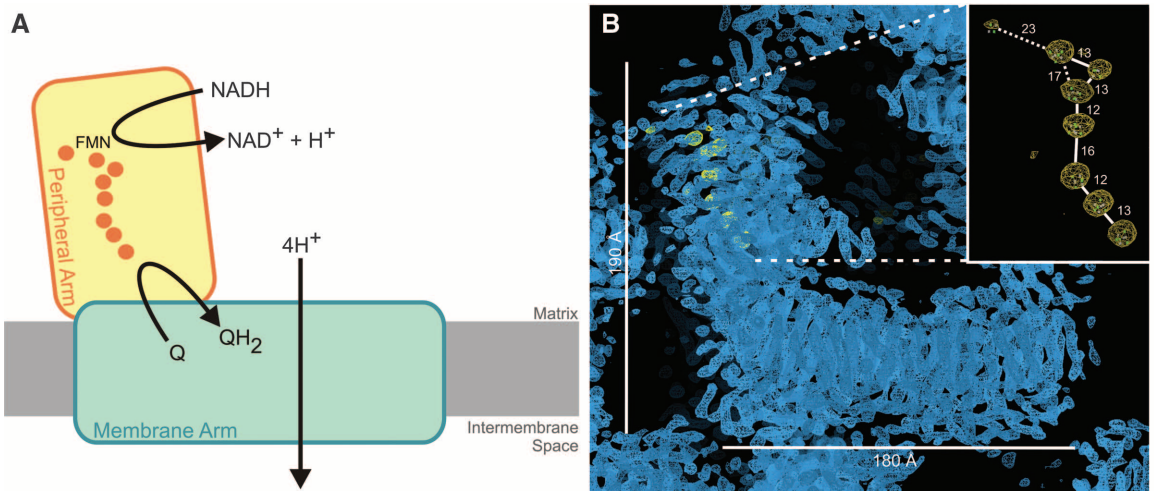


**Fig. 1.** Overall shape and iron-sulfur cluster positions. (**A**) Schematic depiction of overall organization and function of mitochondrial complex I. FMN and a chain of iron-sulfur clusters (orange spheres) in the peripheral arm connect the NADH oxidation site with the ubiquinone (Q) reduction site. The redox reaction is linked to the translocation of four protons across the inner mitochondrial membrane. (**B**) Well-defined electron density corresponding to one molecule of L-shaped complex I shown in side view with the membrane arm displayed horizontally. The anomalous Fourier map contoured at 4.5 σ, indicating the positions of eight iron-sulfur clusters of the peripheral arm, is displayed in yellow and shown enlarged and slightly turned for better visualization of all clusters in the insert. Center-to-center distances are given in angstroms. Solid white lines indicate that these distances are short enough for physiological electron transfer; otherwise, dashed lines are used. The anomalous map is overlayed with cluster positions from the bacterial partial structure.

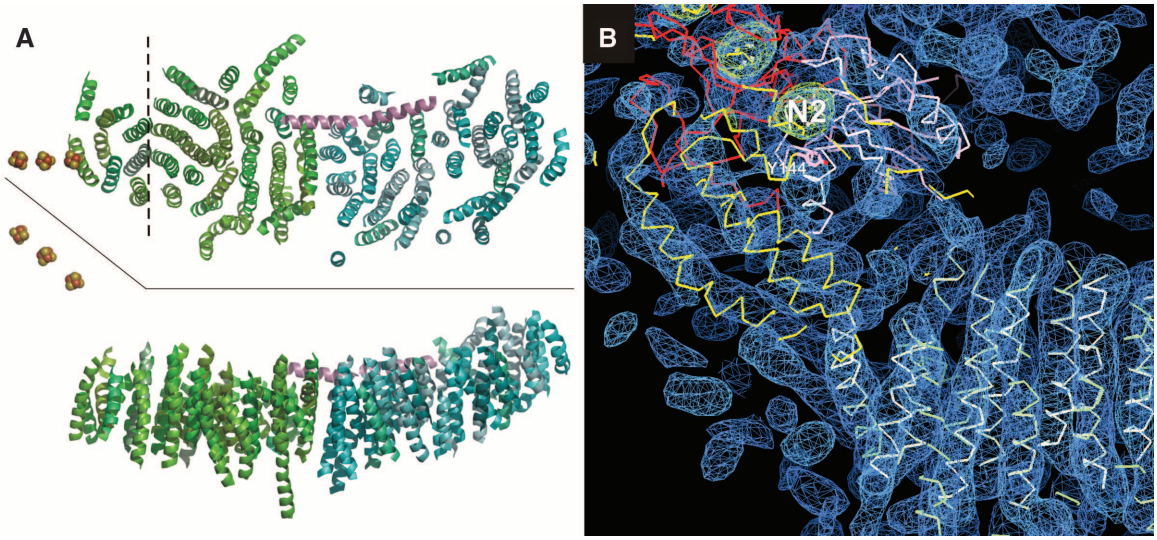


**Fig. 2.** Transmembrane segments and interface of the membrane arm and the peripheral arm. (**A**) Top view from matrix side and side view of the α-helical model of the transmembrane segments (upper and lower panel, respectively) fitted with helices arranged in a proximal (green) and a distal (cyan) domain. The border of the docking area with the peripheral arm is indicated by a dashed line (top). The three iron-sulfur clusters of the Q module are shown in space-filled representation. An extended helical element (magenta) may be critical for energy transmission within the membrane arm. (**B**) Side view of electron density with transmembrane segments including their helical model and the superimposed structure of the bacterial peripheral arm fragment (3IAM). Yellow, 49-kD subunit; pink, PSST subunit; red, TYKY subunit; green, anomalous Fourier map indicating positions of iron-sulfur clusters. The vertical distance from iron-sulfur cluster N2, which is the immediate electron donor to ubiquinone, to the membrane surface is ~30 Å. The conserved tyrosine (Y144) implicated in binding the ubiquinone head group is shown in light purple.

well-defined positions of the iron-sulfur clusters and prominent secondary structure elements revealed that two parts of the peripheral arm form rigid bodies corresponding to the Q and N modules. Compared with the bacterial fragment, the Q and N modules are opened 3° wider and turned slightly, relative to each other. This reorientation does not affect the distances for electron transfer between the two parts of complex I.

For the P module, prediction algorithms and mapping experiments suggest the presence of 17 membrane-integral subunits with more than 70 transmembrane segments (*16*). We modeled 71 α-helical transmembrane segments of different lengths, tilts, and curvatures into continuous elongated electron density features (Fig. 2A). At least two of the latter appear interrupted in the middle of the membrane core, which is suggestive of discontinuous helices that are a hallmark of sodium-proton antiporters and other ion-translocating proteins (*22*). This finding is reminiscent of the homology of subunits ND2, ND4, and ND5 to subunits of bacterial sodium-proton antiporters (*17*). Overall, the side view of the transmembrane segments (Fig. 2A, bottom) reveals a curved shape, with the concave side facing the mitochondrial matrix. This appearance of the membrane arm was also observed for bacterial complex I by EM (*10*, *23*). The extrinsic protein portion on the matrix side largely consists of the peripheral arm and a protrusion at the distal end (Fig. 1B). In contrast, the intermembrane side is characterized by a prominent layer of electron density that is spread over the entire membrane arm. The layer includes well-defined elongated density features that probably represent long surface helices extending parallel to the long axis of the membrane arm. The membrane arm shows two entities of about equal size dividing the P module into a proximal and distal domain (Fig. 2A). They are connected by a narrow, centrally located interface occupying only about half of the width of the membrane arm. The analysis of defined subcomplexes had already suggested a modular architecture of the membrane (*24*), and the proposed proton-translocating subunits ND4 and ND5 can be assigned to the distal P domain.

The driving force for proton translocation must be generated in the peripheral arm from the

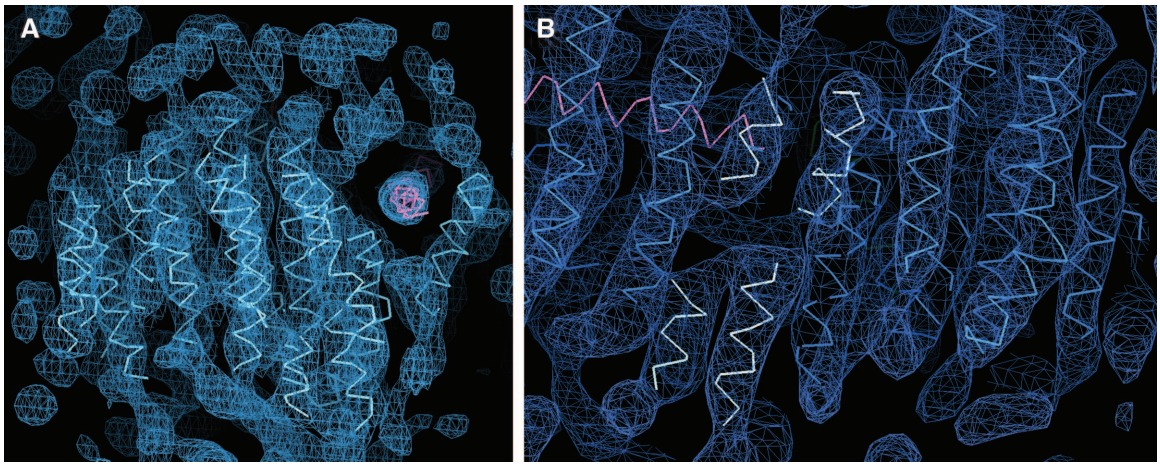


**Fig. 3.** Transmission element connecting the P domains, a putative central component of the proton-pumping machinery. The transmission element, seen as elongated density feature close to the matrix-exposed surface, is fitted with a helical structure (magenta). Connecting the proximal with the distal P domain, this helix may drive proton pumping by conferring conformational coupling. The helical model of the transmembrane segments is shown in blue. (**A**) View in parallel to the transmission element from the distal P domain along the long axis of the membrane arm. (**B**) Partial side view of the distal P domain shows electron density features that reside near the end of the transmission element and resemble discontinuous helix arrangements (light blue) that are a hallmark of ion-translocating proteins.

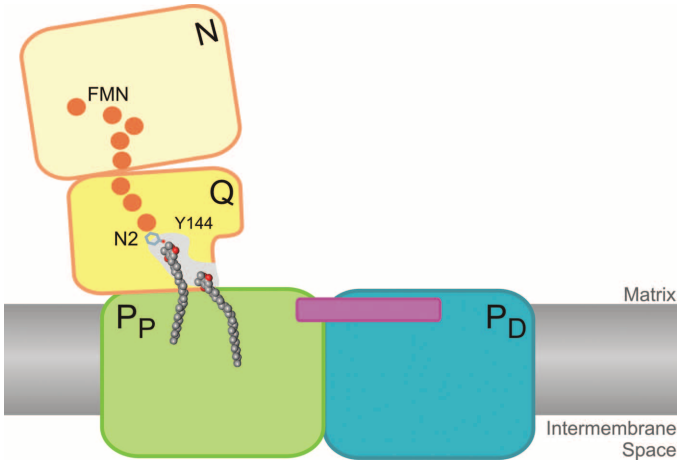


**Fig. 4.** Schematic model of the four functional modules of complex I. A chain of seven iron-sulfur clusters (orange spheres) leads from the N module (light yellow) with FMN as the primary electron acceptor to the ubiquinone reduction site in the Q module (yellow) involving cluster N2 and tyrosine-144. The position of N2 is close to 30 Å above the membrane surface. With the ubiquinone headgroup (space-fill representation) in functional distance to the electron donor at the end of the extended binding cavity (light gray), the hydrophobic isoprenoid side chain will be about half-way out of the core membrane region. This suggests the presence of a hydrophobic access path and excludes direct coupling between redox chemistry in the N and Q modules and vectorial proton translocation by subunits of the proximal ($P_P$, green) and distal ($P_D$, cyan) domains of the P module. An extended transmission element (magenta) forms a bridge across the two domains.

energy released during electron transfer from NADH to ubiquinone. Several lines of evidence suggest that it is the redox chemistry of ubiquinone that triggers the proton-pumping machinery (*16*, *25*, *26*). Thus, the spatial arrangement of the Q and P modules, and the transmission of energy between them, is fundamental to redox-linked proton translocation by complex I.

Critical residues for interaction with ubiquinone and inhibitors are found at the interface of the highly conserved 49-kD and PSST subunits (for complex I subunits, the nomenclature of the bovine heart enzyme is used) of the Q module (*27*–*29*) (fig. S1 and table S1) that are homologous to the large and small subunit of [NiFe] hydrogenase and form the ubiquinone-reducing catalytic core of complex I (*1*). The three iron-sulfur clusters of the Q module provide a precise anchoring point for the superimposition of the bacterial partial structure with respect to the membrane arm. The 49-kD subunit contains a characteristic four-helix bundle that is seen in the experimental electron density map (Fig. 2B). The three iron-sulfur clusters of the Q module line up at an angle of 130 to 140° with respect to the membrane arm (Fig. 1B). In the top view, the vertical projection of this array is centrally oriented in parallel to the long axis of the membrane arm. The 49-kD and PSST subunits dock on the proximal end of the membrane arm (Fig. 2A, top). The main part of the docking site is covered by the 49-kD subunit with its conserved N-terminal β sheet that is oriented toward but outside of the membrane arm surface. A smaller part is composed of parts of the PSST subunit. In the membrane arm, the docking site is bordered by four long, straight, and densely arranged electron density features, indicating a row of four hardly tilted transmembrane helices (Fig. 2A). The contact site has a more open appearance toward subunit PSST, and we suggest that this area provides access for ubiquinone from the phospholipid bilayer.

The last iron-sulfur cluster in the chain, called N2, is the immediate electron donor for ubiquinone. A funnel-like cavity leading from the N-terminal β sheet of the 49-kD subunit toward tyrosine-144, (tyrosine-87 in *Thermus thermophilus*), which is in the immediate vicinity of cluster N2, has been mapped by site-directed mutagenesis (*27*, *28*). It has been shown by detailed structure/function analysis that ubiquinone binds directly to this fully conserved tyrosine (*29*). Measured perpendicular to the membrane plane, cluster N2 resides ~30 Å above the surface of the transmembrane core (Fig. 2B). The distance from the opening of the ubiquinone-binding pocket at the surface of the membrane arm to the electron donor site is ~35 Å. Considering that the binding site for ubiquinone must be at a distance allowing electron transfer of cluster N2, the substrate must diffuse ~25 Å out from the hydrophobic core of the membrane to position the functional head group in the active site. This distance accounts for much of the extremely hydrophobic 40-Å-long side chain of nine isoprenoid units in ubiquinone that may slide over a hydrophobic ramp as previously proposed (*30*, *31*).

This arrangement of the peripheral arm has far-reaching implications for the catalytic mechanism of complex I and is similar to one of the possible orientations (fit 2) determined in a previous study by using single-particle EM (*31*) but differs from that suggested by Sazanov and coworkers (*11*, *23*). The position of the ubiquinone reduction site separate from the transmembrane domain of complex I seems to rule out any mechanism that would use redox-linked proton uptake and release directly for vectorial proton translocation. Rather, the energy released in the redox reactions is transmitted to the proton-pumping machinery via long-range conformational changes (*1*, *16*, *32*). Considering that subunits ND4 and ND5 at the distal end of the membrane arm are

among the prime candidates to harbor proton-translocation sites, distances for energy-transfer reactions of more than 100 Å have to be envisaged. A continuous electron density most likely corresponding to an α helix is laterally associated with the membrane arm embedded in the transmembrane segments near the matrix-facing surface (Fig. 3). With a length of 60 Å oriented in parallel to the long axis of the membrane arm, it extends from the end of the proximal domain about half-way into the distal domain (Fig. 2A). At the proximal end, it is connected by continuous electron density to one of the transmembrane segments in a nearly orthogonal orientation. Strikingly, on the $P_D$ domain side, it terminates close to electron density features resembling a discontinuous helix arrangement, suggesting the presence of a proton-translocation unit (Fig. 3B) (*22*). We propose that this observed connection between the P domains is a critical transmission element within the proton-pumping machinery of complex I.

The modular architecture of complex I as revealed by crystallographic analysis of the complete mitochondrial enzyme is summarized in Fig. 4. In a bipartite functional organization, conformational energy is generated by the redox chemistry occurring in the N and Q modules of the peripheral arm and is transmitted to the two proton-pumping modules of the membrane arm, which are connected by a helical transmission element.

**References and Notes**


1. U. Brandt, *Annu. Rev. Biochem.* **75**, 69 (2006).
2. M. K. F. Wikström, *FEBS Lett.* **169**, 300 (1984).
3. A. Galkin, S. Dröse, U. Brandt, *Biochim. Biophys. Acta* **1757**, 1575 (2006).
4. A. Galkin, U. Brandt, *J. Biol. Chem.* **280**, 30129 (2005).
5. L. Kussmaul, J. Hirst, *Proc. Natl. Acad. Sci. U.S.A.* **103**, 7607 (2006).
6. M. T. Lin, M. F. Beal, *Nature* **443**, 787 (2006).
7. V. Rhein *et al*., *Proc. Natl. Acad. Sci. U.S.A.* **106**, 20057 (2009).
8. H. Fukui, C. T. Moraes, *Trends Neurosci.* **31**, 251 (2008).
9. M. Radermacher *et al*., *J. Struct. Biol.* **154**, 269 (2006).
10. T. Clason *et al*., *J. Struct. Biol.* **169**, 81 (2010).
11. L. A. Sazanov, P. Hinchliffe, *Science* **311**, 1430 (2006).
12. J. M. Berrisford, L. A. Sazanov, *J. Biol. Chem.* **284**, 29773 (2009).
13. M. L. Verkhovskaya, N. Belevich, L. Euro, M. Wikström, M. I. Verkhovsky, *Proc. Natl. Acad. Sci. U.S.A.* **105**, 3763 (2008).
14. D. Esterhazy, M. S. King, G. Yakovlev, J. Hirst, *Biochem.* **47**, 3964 (2008).
15. P. Hinchliffe, L. A. Sazanov, *Science* **309**, 771 (2005).
16. V. Zickermann *et al*., *Biochim. Biophys. Acta* **1787**, 574 (2009).
17. C. Mathiesen, C. Hägerhäll, *Biochim. Biophys. Acta* **1556**, 121 (2002).
18. S. Kerscher, S. Dröse , K. Zwicker, V. Zickermann, U. Brandt, *Biochim. Biophys. Acta* **1555**, 83 (2002).
19. N. Morgner *et al*., *Biochim. Biophys. Acta* **1777**, 1384 (2008).
20. A. Abdrakhmanova *et al*., *Biochim. Biophys. Acta* **1658**, 148 (2004).
21. Materials and methods are available as supporting material on *Science* Online.
22. E. Screpanti, C. Hunte, *J. Struct. Biol.* **159**, 261 (2007).
23. D. J. Morgan, L. A. Sazanov, *Biochim. Biophys. Acta* **1777**, 711 (2008).
24. E. A. Baranova, D. J. Morgan, L. A. Sazanov, *J. Struct. Biol.* **159**, 238 (2007).
25. G. Belevich, L. Euro, M. Wikstrom, M. Verkhovskaya, *Biochem.* **46**, 526 (2007).
26. K. Zwicker *et al*., *J. Biol. Chem.* **281**, 23013 (2006).
27. M. A. Tocilescu, U. Fendel, K. Zwicker, S. Kerscher, U. Brandt, *J. Biol. Chem.* **282**, 29514 (2007).
28. U. Fendel, M. A. Tocilescu, S. Kerscher, U. Brandt, *Biochim. Biophys. Acta* **1777**, 660 (2008).
29. M. A. Tocilescu *et al*., *Biochim. Biophys. Acta* **1797**, 625 (2010).
30. V. Zickermann *et al*., *J. Biol. Chem.* **278**, 29072 (2003).
31. T. Clason, V. Zickermann, T. Ruiz, U. Brandt, M. Radermacher, *J. Struct. Biol.* **159**, 433 (2007).
32. T. Friedrich, *J. Bioenerg. Biomembr.* **33**, 169 (2001).


33. Excellent technical assistance by K. Siegmund and technical support by A. Duchene, F. Streb, and B. Wenzel are gratefully acknowledged. We thank S. Kerscher for his essential contributions regarding all aspects of *Y. lipolytica* genetics and B. Wrzesniewska for testing the impact of antibody fragments to improve crystallization. We are indebted to H. Michel for valuable advice during the initial stages of the project and for his continuous support. We thank the European Synchrotron Radiation Facility and the Swiss Light Source (SLS) for granting beam time, many scientists especially at SLS beamlines X06SA and X10SA for constantly supporting our work, and the staff of the Helmholtz Zentrum für Infektionsforschung (HZI)/Gesellschaft für Biotechnologische Forschung, Braunschweig for large-scale fermentation of *Y. lipolytica*. Funding by the Deutsche Forschungsgemeinschaft (SFB 472 Projects P2 and P17) is gratefully acknowledged. This study was supported by the Excellence Initiative of the German Federal and State Governments (EXC 115 and EXC 294). Electron density maps are available on request.


**Supporting Online Material**

www.sciencemag.org/cgi/content/full/science.1191046/DC1
Materials and Methods
Fig. S1
Tables S1 and S2
References

16 April 2010; accepted 10 June 2010
Published online 1 July 2010;
10.1126/science.1191046
Include this information when citing this paper.

# An Electronic Bus Bar Lies in the Core of Cytochrome $bc_1$

**Monika Świerczek,[1] Ewelina Cieluch,[1] Marcin Sarewicz,[1] Arkadiusz Borek,[1] Christopher C. Moser,[2] P. Leslie Dutton,[2] Artur Osyczka[1]***

**The ubiquinol–cytochrome c oxidoreductases, central to cellular respiration and photosynthesis, are homodimers. High symmetry has frustrated resolution of whether cross-dimer interactions are functionally important. This has resulted in a proliferation of contradictory models. Here, we duplicated and fused cytochrome b subunits, and then broke symmetry by introducing independent mutations into each monomer. Electrons moved freely within and between monomers, crossing an electron-transfer bridge between two hemes in the core of the dimer. This revealed an H-shaped electron-transfer system that distributes electrons between four quinone oxidation-reduction terminals at the corners of the dimer within the millisecond time scale of enzymatic turnover. Free and unregulated distribution of electrons acts like a molecular-scale bus bar, a design often exploited in electronics.**

Figure 1 shows a bacterial ubiquinol–cytochrome c oxidoreductase (*1*), often called cytochrome $bc_1$, displaying homodimeric core subunit structure typical of respiratory and photosynthetic electron transfer systems (*2*, *3*). It is well established that adjacent cofactors in each monomer serve to separate electronic charge across the membrane in the catalytically relevant microsecond-to-millisecond electron transfer process (*4*, *5*). However, high structural, spectroscopic, and electrochemical symmetry between the monomers of the dimer has confounded efforts to determine whether a functional electron-transfer connection exists between monomers. At the distances displayed in Fig. 1, calculations show that electron-tunneling times between cofactors in different monomers are much slower than the physiologically relevant time scale, except for tunneling between the two $b_L$ hemes. Electron tunneling across the 13.9 Å separating these two hemes is calculated to be in the 0.025- to 0.25-ms range (*5*), slightly faster than the measured 0.5- to 5.0-ms physiological turnover time. However, electron-tunneling theory itself (*6*, *7*) provides only an upper limit for the rate of electron transfer between redox cofactors. Many electron transfers in oxidoreductases are limited not by electron tunneling but by slower coupled events of chemistry, conformational change, or motion (*8*, *9*). Indeed, many models have been proposed for ubiquinol–cytochrome c oxidoreductases that include just such regulation of electron transfer within or between monomers (*10*–*15*) or even strict electronic isolation of monomers (*16*). Given the inherent tunneling speed, a relatively small amount of coupling of this electron tunneling to chemical or conformational events could effectively regulate interaction between monomers or even isolate them (*10*–*16*).

To resolve the underlying dimer engineering, we broke the symmetry of the cytochrome $bc_1$ homodimer from *Rhodobacter capsulatus* shown

[1]Department of Biophysics, Faculty of Biochemistry, Biophysics and Biotechnology, Jagiellonian University, Kraków, Poland. [2]The Johnson Research Foundation, Department of Biochemistry and Biophysics, University of Pennsylvania, PA 19104, USA.

*To whom correspondence should be addressed. E-mail: artur.osyczka@uj.edu.pl